Korea-Australia Rheology Journal
Vol. 16, No. 3, September 2004 pp. 117-128

Vortex behavior in the inertial flow of viscoelastic fluids past a confined cylinder

Ju Min Kim[1], Chongyoup Kim[1], Changkwon Chung, Kyung Hyun Ahn and Seung Jong Lee*
School of Chemical Engineering, Seoul National University, Seoul 151-744, Korea
[1]Department of Chemical and Biological Engineering, Korea University, Seoul 136-701, Korea
(Received June 7, 2004; final revision received August 3, 2004)

Abstract

The effect of molecular parameters on the steady vortex behaviors in the inertial viscoelastic flow past a cylinder has been investigated. FENE-CR model was considered as a constitutive equation. A recently developed iterative solution method (Kim *et al.*, (in press)) was found to be successfully applicable to the computation of inertial viscoelastic flows. The high-resolution computations were carried out to understand the detailed flow behaviors based on the efficient iterative solution method armed with ILU(0) type preconditioner and BiCGSTAB method. The discrete elastic viscous split stress-G/streamline upwind Petrov Galerkin (DEVSS-G/SUPG) formulation was adopted as a stabilization method. The vortex size decreased as elasticity increases. However, the vortex enhancement was also observed in the case of large extensibility, which means that the vortex behavior is strongly dependent upon the material parameters. The longitudinal gradient of normal stress was found to retard the formation of vortex, whereas the extensional viscosity played a role in the vortex enhancement. The present results are expected to be helpful for understanding the inertial vortex dynamics of viscoelastic fluids in the flow past a confined cylinder.

Keywords : vortex behavior, flow past a confined cylinder, FENE-CR, DEVSS-G/SUPG, iterative solver

1. Introduction

Flow around a cylinder problem has been intensively studied as a benchmarking problem in the field of viscoelastic flow simulation. Though they are practically important, however, the detailed flow characteristics have not yet been fully understood due to the difficulty in the numerical computation of very thin stress boundary layer and singular behavior. Recently, Dou and Phan-Thien (2003) compiled the issues related to the viscoelastic flow around a cylinder; 1) variation of drag coefficient, 2) upstream or downstream shift of streamline and 3) so called "negative wake" phenomenon. For the low Reynolds number flow, there seems to be a consensus about the drag coefficient. It shows an initial decrease and a recovery with increasing elasticity (Huang and Feng, 1995). However, there is a wide discrepancy in the prediction of streamline shift among previous theoretical and experimental results. Ultman and Denn (1971) showed an upstream streamline shift by theoretical analysis and visualization with aqueous polymer solution. Broadbent and Mena (1974) found no discernable difference from Newtonian case, and Mena and Caswell (1974) predicted the downstream shift. Koniuta *et al.* (1980) found that the upstream shift is more obvious with increasing *We* in front of the cylinder, while the wake is much broader and the velocities are slower than the Newtonian case in the rear of the cylinder. McKinley *et al.* (1993) showed that the velocity profile is nearly independent of *We* at the front of the cylinder, whereas the velocity shifts downstream in the wake region with increasing elasticity. They also showed the same trend by numerical simulation using FENE-CR model (Chilcott and Rallison, 1988). Very recently, Dou and Phan-Thien (2003) predicted that the flow is shifted downstream for UCM and Oldroyd-B models in creeping flow, whereas the streamline for PTT monotonically shifts upstream behind the cylinder. For FENE-CR fluid, they showed that the behavior is similar to PTT at low value of L (extensibility), and its behavior is similar to Oldroyd-B model for high value of L except the velocity overshoot that occurs further downstream, which means that the downstream or upstream shift strongly depends on the material parameters.

Hassager (1979) found so-called "negative wake" which occurs in the viscoelastic flow behind a moving object or a bubble. "Negative wake" denotes a velocity overshoot in the reference frame of fixed object. Chilcott and Rallison (1998) did not find any overshoot in the axial velocity using their constant shear viscosity model (FENE-CR

*Corresponding author: sjlee@plaza.snu.ac.kr

model) and explained that "negative wake" arises from the combined effect of shear-thinning and large extensibility. Although McKinley *et al.* (1993) performed extensive experiments with Boger fluid, they did not find an overshoot up to flow instability. Arigo and McKinley (1998) showed by experiments that "negative wake" could always occur for shear thinning fluid in flow around a sphere. However, "negative wake" was observed using FENE-CR model with low extensibility by Satrape and Crochet (1994). Dou and Phan-Thien (2003) investigated the influence of parameters of constitutive equations on the negative wake and concluded that a lower extensional viscosity will promote the generation of a negative wake, which supports the importance of extensional viscosity as Bush (1994) pointed out. Harlen (2002) explained the mechanism of negative wake such that the "negative wake" is formed by the relaxation of shear stress generated near the side of a sphere and this force is competing with the extensional stress generated in the extensional flow at the rear of the sphere. Dou and Phan-Thien (2004) proposed a critical *We* for PTT, FENE-CR, FENE-P and Giesekus models by analyzing the velocity profile along the centerline of the wake region.

The three issues related to the cylinder problem have been extensively investigated, however, they were mainly restricted to inertialess flows. The vortex dynamics generated behind the cylinder is not well understood in inertial flows in spite of its practical importance. In literatures, there exist several experimental reports on inertial vortex dynamics in the flow around a sphere or cylinder. James and Acosta (1970) showed a drag increase and reduced heat transfer coefficient for large values of Reynolds number. Adachi *et al.* (1977; 1978) showed that the vortex size decreases with elasticity. On the other hand, Koniuta *et al.* (1980) showed that the wake is much broader, however, they did not directly show the behavior of vortex size.

As for numerical simulation of inertial flows, there are several results with the continuum-based constitutive equations. Pilate and Crochet (1977) predicted with a second-order fluid that the inertial vortex is elongated behind the cylinder compared to the Newtonian case. Townsend (1980) showed the same trend using four-constant Oldroyd model. Hu and Joseph (1990) using UCM model showed that the streamlines around the cylinder and recirculation zone detach from the cylinder and the gap among the streamlines becomes larger as elasticity increases, which results in the increase of vortex size. Huang and Feng (1995) showed that the axial velocity shifts downstream for Oldroyd-B model in the uniform flow. However, there seems to be no discernable difference in vortex size in their results. Matallah *et al.* (1998) showed that the vortex size strongly depends on numerical schemes. Later, Wapperom and Webster (1999) revisited the same problem with a finite volume/element hybrid scheme. According to their results, no vortex enhancement was detected up to numerical failure and the downstream shift was reproduced. Recently, Oliveira (2001) conducted the transient numerical simulation of vortex shedding past a cylinder for Newtonian and FENE-CR fluids. He showed that the frequency of vortex shedding is attenuated by elasticity of the fluid and the size of vortex behind the cylinder is extended. He related it to the previous experimental works of Cressman *et al.* (2001), and explained in terms of the restabilization effect of viscoelasticity.

However, there is few numerical simulation with the molecule-based constitutive equations and the influence of molecular parameters has not yet been realized. In this work, we focus on the flow behavior of FENE-CR fluid (Chilcott and Rallison, 1988) past a confined cylinder and investigate the influence of elasticity and material parameters on the inertial vortex.

Since it is known that the flow simulation of viscoelastic flow past a confined cylinder is difficult due to the very thin boundary layer at both cylinder wall and wake region, a very refined mesh should be used in the high gradient region of extra stress to capture the detailed behaviors of the flow fields. In this work, DEVSS-G (discrete elastic viscous split stress-G)/SUPG (streamline upwinding Petrov Galerkin) scheme was implemented as a stabilization scheme. The high-resolution computation was applied to inertial flow based on the efficient iterative solution method (Kim *et al.*, (in press)) which is composed of modified adaptive incomplete LU(0) preconditioner and BiCG-STAB (bi-conjugate gradient stabilized) method (van der Vorst, 1992). In our previous work, solutions were obtained for inertialess flow and the application to inertial flow will be presented in this paper.

2. Governing Equations and boundary conditions

We consider the momentum equation including inertia with incompressibility constraint, and FENE-CR model is employed as a constitutive equation. FENE-CR model predicts constant shear viscosity, shear-thinning of first normal stress difference coefficient, and controlled elongational viscosity.

$$Re(\boldsymbol{u}\cdot\nabla\boldsymbol{u}) = -\nabla p+\nabla\cdot\boldsymbol{\tau} \tag{1}$$

$$\nabla\cdot\boldsymbol{u} = 0 \tag{2}$$

$$\boldsymbol{\tau}_p+\frac{We}{f}(\boldsymbol{u}\cdot\nabla\boldsymbol{\tau}_p-(\nabla\boldsymbol{u})^T\cdot\boldsymbol{\tau}_p-\boldsymbol{\tau}_p\cdot(\nabla\boldsymbol{u})) = \beta((\nabla\boldsymbol{u})+(\nabla\boldsymbol{u})^T),$$

$$f=\frac{L^2+(We/\beta)tr(\boldsymbol{\tau}_p)}{L^2-3} \tag{3}$$

In the above equations, β is the viscosity ratio of polymer (η_p) and solution (η_0), the velocity $\boldsymbol{u}$ is scaled with a characteristic velocity U, the stress tensor $\boldsymbol{\tau}$ and pressure p are

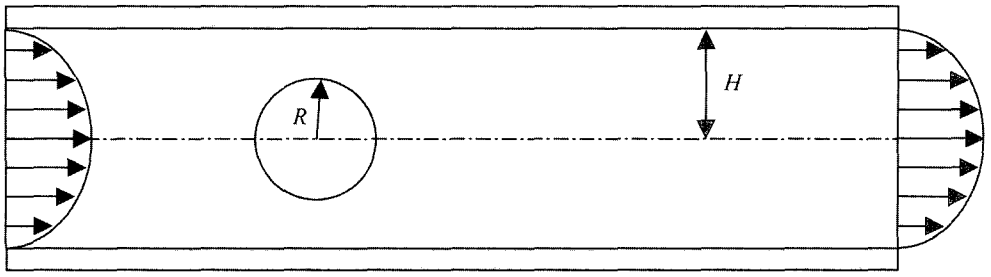

(a) Flow Condition

Fig. 1. Schematic diagram of flow past a confined cylinder.

scaled with $\eta_0 U/H_c$, where H_c is the characteristic length (radius of cylinder). Extra stress tensor τ comprises of Newtonian stress contribution τ_s and polymer contribution τ_p. *Re* denotes the Reynolds number that is defined by $H_c U\rho/\eta_0$ and *We* is the Weissenberg number which stands for $\lambda U/H_c$, where ρ is density, η_0 denotes viscosity and λ stands for the relaxation time. The Poiseuille flow condition was assumed as shown in Fig. 1. In Poiseuille flow boundary condition, the unperturbed velocity profile is parabolic and its average velocity is $<u>$.

2.1. Boundary conditions

No slip boundary condition was imposed on the cylinder wall as well as upper and lower plates. Fully developed boundary conditions of extra stresses and velocity were imposed on the inlet. Fully developed velocity fields were imposed on the outlet and boundary condition for extra stress is not necessary on the outlet. The fully developed velocity field and extra stress can be denoted by

$$u = \frac{3}{2}\langle u\rangle\left(1-\left(\frac{y}{H}\right)^2\right), \quad v=0 \tag{4}$$

$$\tau_{xx} = 2\beta We\left(\frac{\partial u}{\partial y}\right)^2\frac{1}{g}, \quad g = \frac{L^2+\sqrt{L^4+8(L^2-3)We^2\left(\frac{\partial u}{\partial y}\right)^2}}{2(L^2-3)} \tag{5}$$

$$\tau_{yy} = 0 \tag{6}$$

$$\tau_{xy} = \beta\left(\frac{\partial u}{\partial y}\right) \tag{7}$$

where $\langle u\rangle$ is the average velocity of the upstream and H is the half of the channel height. The aspect ratio of the half channel height to cylinder radius was fixed to two, and the characteristic velocity U was set to $\langle u\rangle$.

3. Numerical method

In this study, the velocity, pressure, extra stress and velocity gradient tensor were approximated with Lagrangian basis functions as shown in Eq. 8. The computational domain Ω was discretized into quadrilateral finite elements R_e so that $\Omega=\cup R_e$ and $\varnothing=\cap R_e$.

$$\boldsymbol{u} = \sum_i \psi_i u_i, \quad p = \sum_i \phi_i p_i$$

$$\boldsymbol{S} = \sum_i \phi_i S_i, \quad \boldsymbol{G} = \sum_i \phi_i G_i \tag{8}$$

where $\boldsymbol{S}$ denotes τ_p and ϕ_i and ψ_i are the bilinear and biquadratic basis functions, respectively.

The weak forms of Eqs. (1), (2), (3), (8) with DEVSS-G stabilization formulation are

$$\langle Re(\boldsymbol{u}\cdot\nabla\boldsymbol{u});\psi\rangle+\langle -p\boldsymbol{I}+(\nabla\boldsymbol{u}+(\nabla\boldsymbol{u})^T)+\boldsymbol{S}-\beta(\boldsymbol{G}+(\boldsymbol{G})^T);\nabla\psi\rangle$$
$$= \langle\langle(-p\boldsymbol{I}+(\nabla\boldsymbol{u}+(\nabla\boldsymbol{u})^T)+\boldsymbol{S}-\beta(\boldsymbol{G}+(\boldsymbol{G})^T))\cdot\boldsymbol{n};\psi\rangle\rangle \tag{9}$$

$$\langle\nabla\cdot\boldsymbol{u};\phi\rangle = 0 \tag{10}$$

$$(\boldsymbol{G}-\nabla\boldsymbol{u};\phi) = \boldsymbol{0} \tag{11}$$

$$\left\langle \boldsymbol{S}+\frac{We}{f}(\boldsymbol{u}\cdot\nabla\boldsymbol{S}-(\boldsymbol{G})^T\cdot\boldsymbol{S}-\boldsymbol{S}\cdot\boldsymbol{G})-\beta(\boldsymbol{G}+(\boldsymbol{G})^T);\phi\right\rangle = \boldsymbol{0} \tag{12}$$

$$f = \frac{L^2+(We/\beta)tr(\boldsymbol{S})}{L^2-3}$$

where $\boldsymbol{n}$ stands for the outward normal vector at the boundary and $\boldsymbol{I}$ is the unit tensor. In the above equations, symbols $<;>$ and $<<;>>$ denote domain integral and boundary surface integral, respectively. In this work, the modified streamline upwind/Petrov-Galerkin (SU/PG) of Fan and Crochet (1995) was consistently applied to the constitutive equation. In the SU/PG method, standard weight function was modified as follows:

$$\phi_s = \phi+\bar{k}w\cdot\nabla\phi \tag{13}$$

where ϕ_s is the modified weight function and ϕ is the standard bilinear interpolation function. The overall nonlinear equations were linearized using Newton-Raphson method. The convergence criterion for Newton method was set to the L_1 of relative error between two steps less than 10^{-4}. The linear equations of Newton Raphson step were solved by incomplete LU(0) type preconditioner and BiCGSTAB method (van der Vorst, 1992), whose

Table 1. Mesh information

Mesh	Number of finite elements	Number of nodes	Total DOF	Δx at (7,0)	Δy at (7,0)
UM1	6,681	27,320	110,472	0.01000	0.00904
UM2	15,822	64,466	260,220	0.00158	0.00188
UM3	31,671	128,046	514,908	0.00044	0.00052

detailed description will be shown in the separate paper (Kim *et al.*, (in press)). In the solution process of linear equations, the convergence criterion was set to the L_2 norm of residual less than 10^{-10} in BiCGSTAB solver.

4. Results and discussion

Three different meshes were used in this work and their detailed information is presented in Table 1. The magnified meshes are also shown in Fig. 2. They are composed of rectangular finite elements as mentioned in the previous section. As it is of unstructured type, we can increase the computational efficiency by locally refining the order of mesh, and the resolution of mesh was significantly enhanced especially at the rear of the cylinder. All computations were performed using the identical computational domain with Caola *et al.* (1999). The center of cylinder was set to (6,0), the front length 6R and the rear length 12R (See Fig. 1). As denoted in Table 1, (Δx, Δy) was used as a parameter which represents the smallest mesh size at the rear of the cylinder, and was reduced from $O(10^{-2} \times R)$ to $O(10^{-3} \times R)$. The finest mesh in this study has over 30,000 elements and over 500,000 degree of freedoms. It typically took 1~2 hours to obtain the converged solution for Mesh III on a single 2.4 GHz Pentium IV® PC with 2GB main memory. The maximum convergence depends on the Reynolds number, viscosity ratio (β) and extensibility (L^2); the limiting *We* was restricted to 2.5 at L^2=100, β=0.41 and *Re*=10, for example. The maximum

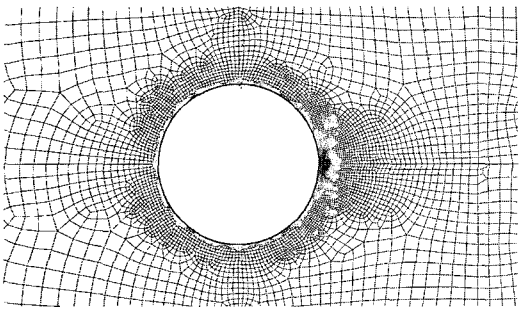

(a) UM1

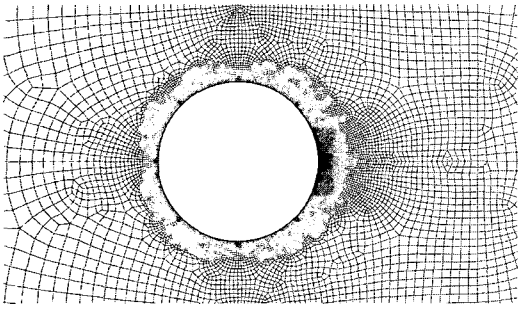

(b) UM2

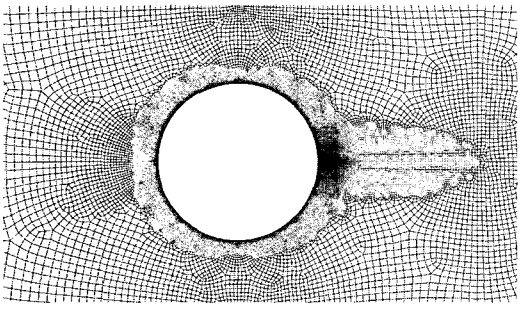

(c) UM3

Fig. 2. Mesh configurations.

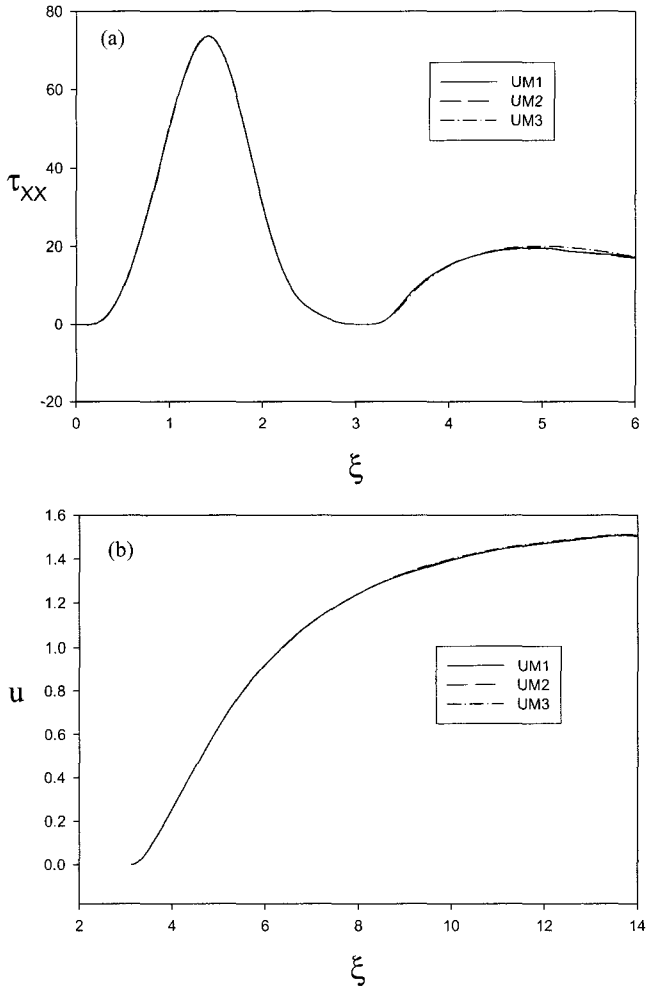

Fig. 3. Mesh refinement test: (a) longitudinal normal stress and (b) velocity profiles.

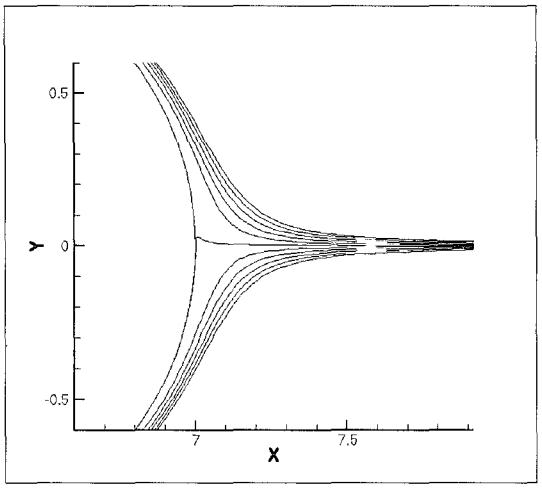

(a) UM1

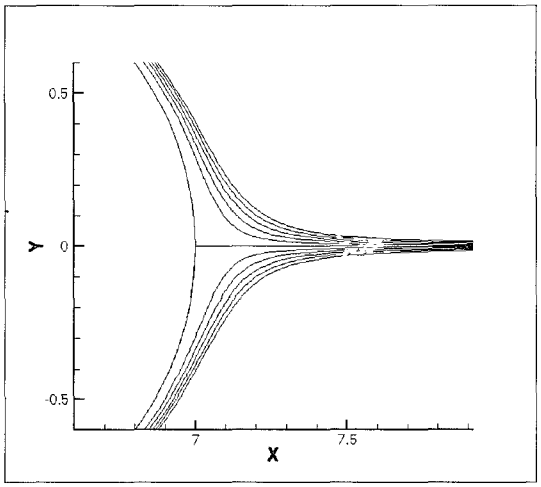

(b) UM2

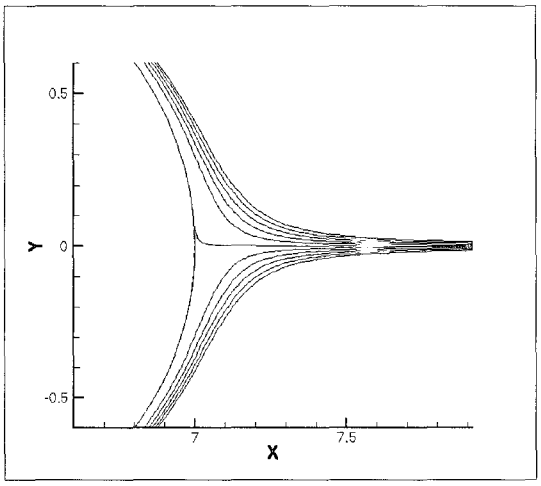

(c) UM3

Fig. 4. Streamlines ($-0.004 \leq \psi \leq 0.004$, $\Delta\psi$=8e-4) at the rear of the cylinder when We=5, Re=10, L^2=100 and β=0.41.

attainable We was reduced as L^2 increases. The mesh refinement test was performed when Re=10, L^2=100, β =0.41 and We=5. The extra stress and velocity in the wake region are plotted along the cylinder wall and centerline in Fig. 3. In the figure, ξ was defined along the cylinder wall and downstream centerline such that its value is 0 at the front stagnation point and π at the rear stagnation point. The extra stress and velocity profiles of different meshes are almost identical. In Fig. 4, the streamlines are also shown with varying meshes. The solutions are independent of the discretization level, which means a good mesh convergence. Hence, all computations have been conducted with Mesh III afterwards.

Caola *et al.* (2001) would be the first who carried out high-resolution finite element computation of viscoelastic fluid flows using a parallel iterative solution method, however, their formulation was restricted to inertialess flow. The present solution method has no limit in taking inertia into account and this study will be the first attempt to show high-resolution computation of inertial flow in computational rheology.

First, the effect of elasticity was investigated in case of Re=10 and L^2=100. In this work, β was set to 0.41 or 0.1. β=0.41 was suitable for Boger fluid of MIT group (McKinley *et al.*, 1993) and used by Dou and Phan-Thien (2003) and Liu *et al.* (1998). Viscosity ratio β=0.1 was used for dilute polymer solutions and this value is close to what Oliveira (2001) used for vortex shedding simulation (β =0.091). As shown in Fig. 5, the vortex is getting small and finally disappears at the same viscosity ratio (β=0.41) as elasticity increases. This tendency is quite different from the previous results with the Oldroyd-B model (Pilate and Crochet, 1977; Townsend, 1980; Hu and Joseph, 1990; Matallah *et al.*, 1998; Wapperom and Webster, 1999), where they reported the growth of vortex size or no vortex enhancement. Longitudinal normal stress component and velocity profile at Re=0 are presented in Fig. 6 along the cylinder wall and centerline. For the longitudinal extra stress field, the extra stress at both cylinder and wake region increases and saturates to the specific profile as We increases. The saturation of longitudinal extra stress at the cylinder wall was also observed in creeping flows of Oldroyd-B model (Alves *et al.*, 2001; Fan *et al.*, 1999). Contrary to our results, the extra stress was shown to monotonically increase in the wake region (Alves *et al.*, 2001; Fan *et al.*, 1999) and the saturation of the present results can be attributed to finite extensibility of the FENE-CR model we have used. For velocity fields, there exist quite different behaviors in two regions, recirculation zone and downstream zone away from the recirculating zone. There are two stagnation points in focus; one at the rear cylinder wall and the other between the recirculating zone and downstream flow field along the centerline. The velocity monotonically shifts upstream in the recirculating zone, whereas a reversal of velocity shift occurs around We=0.5 away from the recirculating region, that is, the velocity

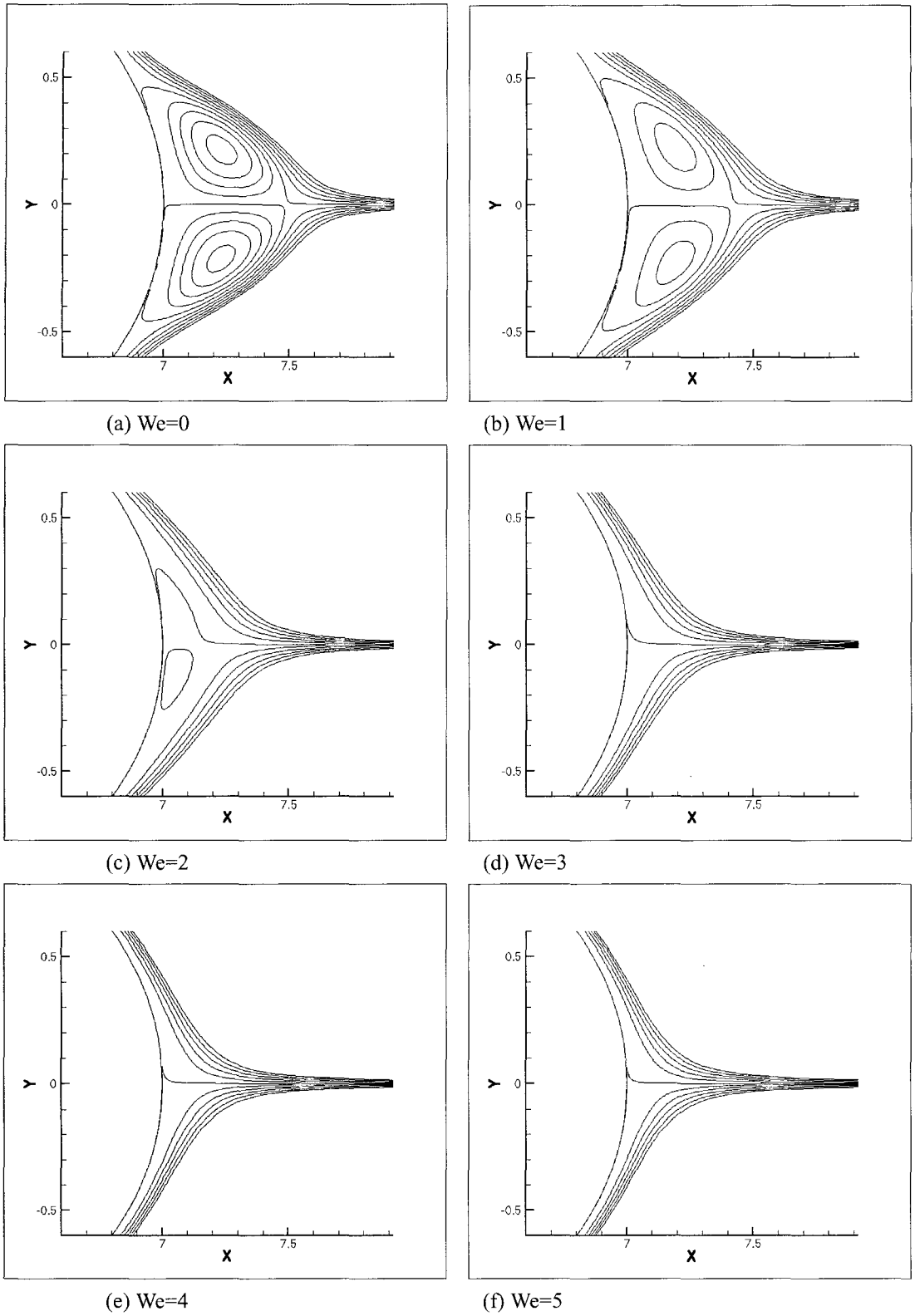

Fig. 5. Streamlines ($-0.004 \leq \psi \leq 0.004$, $\Delta\psi$=8e-4) at the rear of the cylinder when Re=10, L^2=100 and β=0.41 with UM3.

shifts upstream up to *We*=0.5 and shifts downstream over *We*=0.5 in the downstream velocity field. The reversal of velocity shift was also observed in creeping flow simulation of Dou and Phan-Thien (2003) who found the same phenomenon for UCM, Oldroyd-B, FENE-CR with large value of L^2=100 and β=0.9 in uniform flow condition. In

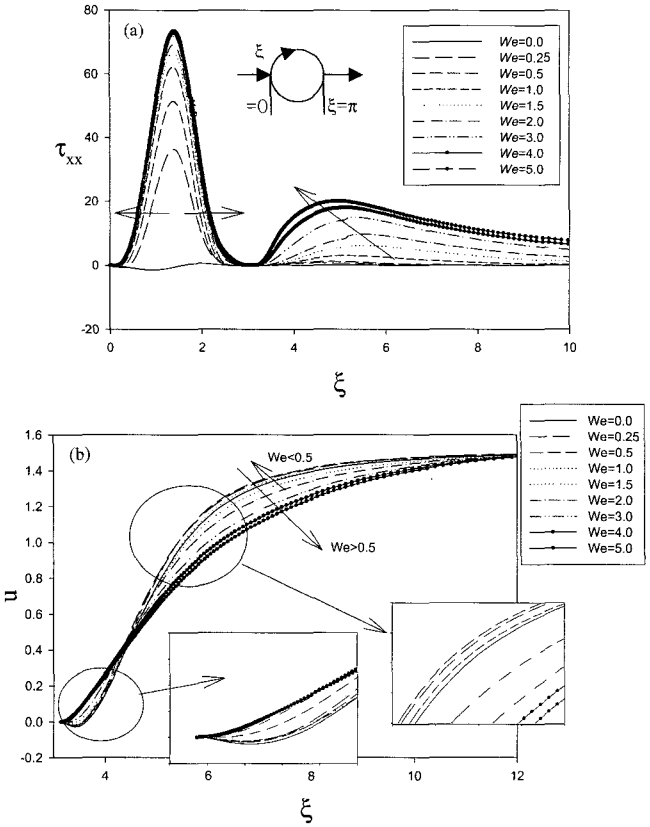

Fig. 6. Longitudinal normal stress component and velocity profiles when Re=10, β=0.41, L^2=100: (a) longitudinal normal stress component and (b) velocity profiles.

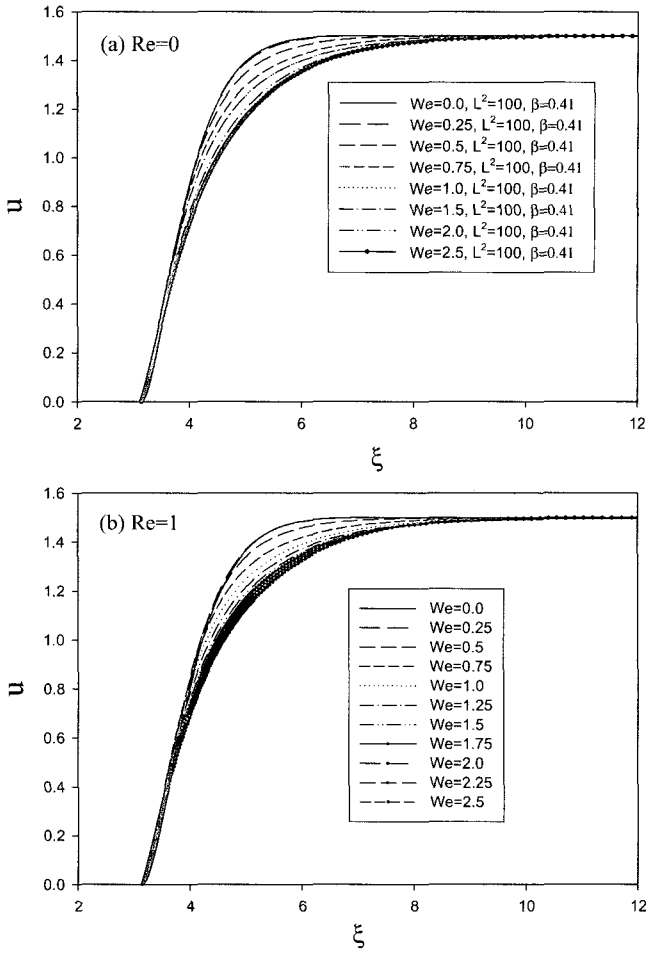

Fig. 7. Velocity profiles; (a) Re=0, β=0.41, L^2=100, (b) Re=1, β=0.41, L^2=100.

Fig. 7, the axial velocity profiles are compared at different Re. When Re is between 0 and 1, the reversal of velocity shift was not observed and the velocity monotonically shifted downstream in contrast to Re=10. So, the reversal of velocity shift depends on Re, material parameters and flow conditions.

The mechanism of vortex shrinkage seems to be complex due to the viscoelastic effect arising from contraction-to-expansion and elongational flow along the centerline after stagnation point. As can be imagined in Fig. 8, the acceleration of fluid element (rapid increase of velocity) results in the reduction of vortex and the deceleration (slower increase of velocity) produces vortex enhancement. In Poiseuille flow condition, the channel flow between cylinder wall and plates can be considered as a contraction flow and the flow from the cylinder to downstream region can be regarded as an expansion flow. Therefore, the flow around a confined cylinder can be envisaged as a contraction-to-expansion flow. The developed extra stress between cylinder wall and the plates relaxes in the downstream zone. Baloch *et al.* (1996) extensively performed numerical simulations using Phan-Thien Tanner model for expansion and contraction flows in both 2D and 3D geometries, and showed that the corner vortex shrinks as elasticity increases,

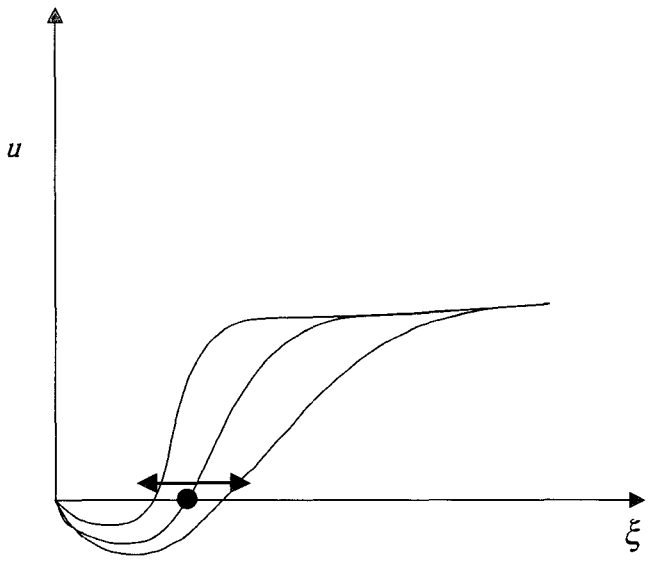

Fig. 8. A schematic diagram for the variation of vortex size depending on the acceleration or retardation of fluid elements near the stagnation point between the recirculating zone and downstream flow field along the centerline.

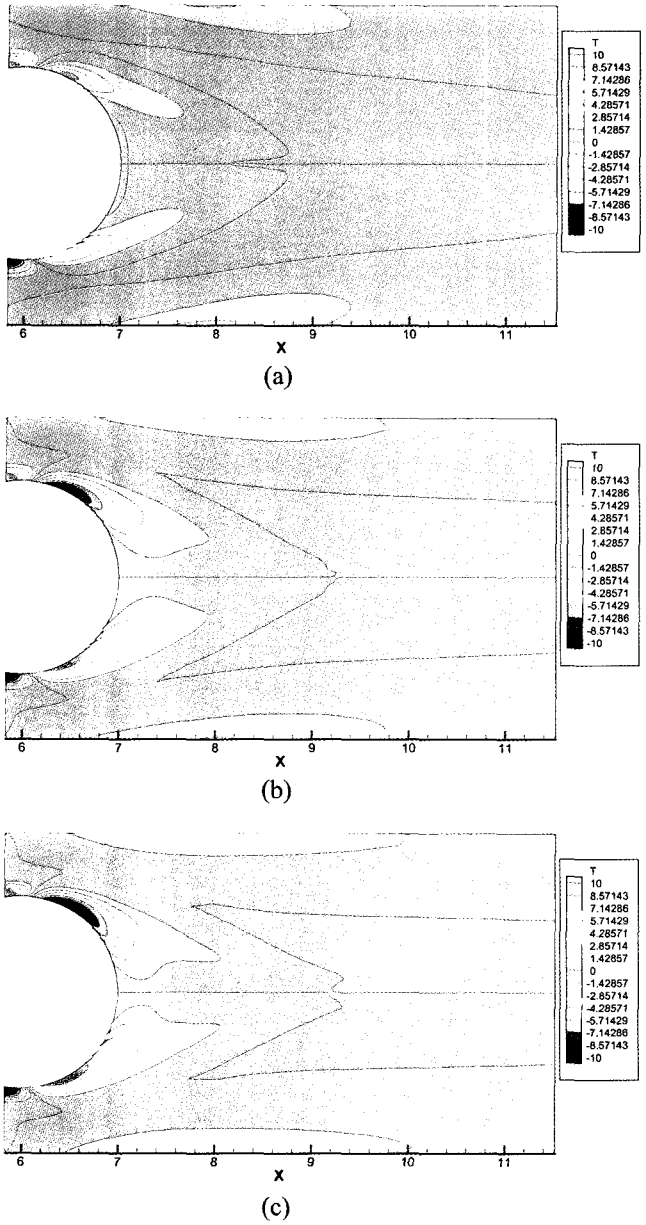

Fig. 9. Shear stress contours; (a) We=1, β=0.41, L^2=100, (b) We=3, β=0.41, L^2=100, (c) We=5, β=0.41, L^2=100.

which seems to be similar to the vortex shrinkage of the present study. However, as there exists a strong extensional flow behind the cylinder along the centerline in the flow around a confined cylinder in contrast to contraction-to-expansion flow, the extensional flow property also plays an important role. According to Harlen (2002), the acceleration of fluid element can be enhanced or retarded by the forcing term, which is defined as follows.

$$f_x = \frac{\partial \tau_{xx}}{\partial x} + \frac{\partial \tau_{xy}}{\partial y} \tag{14}$$

In this equation, $\partial \tau_{xx}/\partial x$ is always positive and $\partial \tau_{xy}/\partial y$ is negative in the recirculating zone. As shown in Fig. 6, the recirculating zone exists between $\xi = \pi$ and ξ=4 (x=7.86), where the longitudinal gradient of normal stress is always positive, whereas $\partial \tau_{xy}/\partial y$ has negative value as shown in Fig. 9. Therefore, it is predicted that the acceleration of fluid element is enhanced or retarded by the competition of $\partial \tau_{xx}/\partial x$ and $\partial \tau_{xy}/\partial y$. The reduction of vortex size seems to originate from positive longitudinal gradient of normal stress that is dominant over negative circumferential gradient of shear stress. However, the velocity profile from the cylinder wall to fully developed zone strongly depends on the extensional viscosity. Both velocity and velocity gradient vanish at the cylinder wall stagnation point, however, the velocity gradient or elongational rate has finite value at the stagnation point between the recirculating zone and developing downstream flow, as shown in Fig. 6(b). The extensional viscosity may play a role in retarding the acceleration of the fluid element at the stagnation point between recirculating zone and developing downstream. Therefore, the combined effect of elasticity convecting between cylinder wall and plates, normal stress and elongational viscosity should be considered together to explain the complex vortex behavior behind the cylinder.

To investigate the effect of elongational viscosity, we performed the computation with two extensibility parameters (L^2=100 and 1000) at constant viscosity ratio (β=0.1). We could obtain converged solutions up to high We of 7 when β was set to 0.1 and L^2=100. The streamlines are presented in Fig. 10 and 11. Velocity and longitudinal extra stress profiles for L^2=100 are also shown in Fig. 12, and the velocity profiles for L^2=1000 are shown in Fig. 13, where Fig. 13(b) is the magnified picture of the circled region in Fig. 13(a). The tendency of overall reduction of vortex size was reproduced. However, the diminishing tendency of vortex size for β=0.1 is weaker than β=0.41. That is, the vortex size is less sensitive to We at low viscosity ratio. The dependency of vortex size on β and L^2 is shown in Fig. 14, where we define the vortex size as the longitudinal length of the recirculating zone. Despite the overall diminishing tendency of the vortex size, there is a slight increase of vortex size up to We=1 for L^2=1000 (Fig. 14). We can explain it by the role of elongational viscosity at the stagnation point between recirculating zone and developing downstream flow. Large elongational viscosity retards the acceleration of the fluid element, which results in the increase of vortex size, as shown in Fig. 8. Since the level of extensional viscosity is higher for L^2=1000 than L^2=100, it is obvious that the acceleration of fluid element is retarded for L^2=1000 and the vortex size increases. However, as the region of vortex enhancement is restricted to small range, the overall diminishing tendency is also reproduced for L^2=1000. From the vortex dynamics mechanism and corresponding numerical observations, the previous vortex enhancement (Huang and Feng, 1995; Matallah *et al.*, 1998) seems to be a subset of the present solutions, and

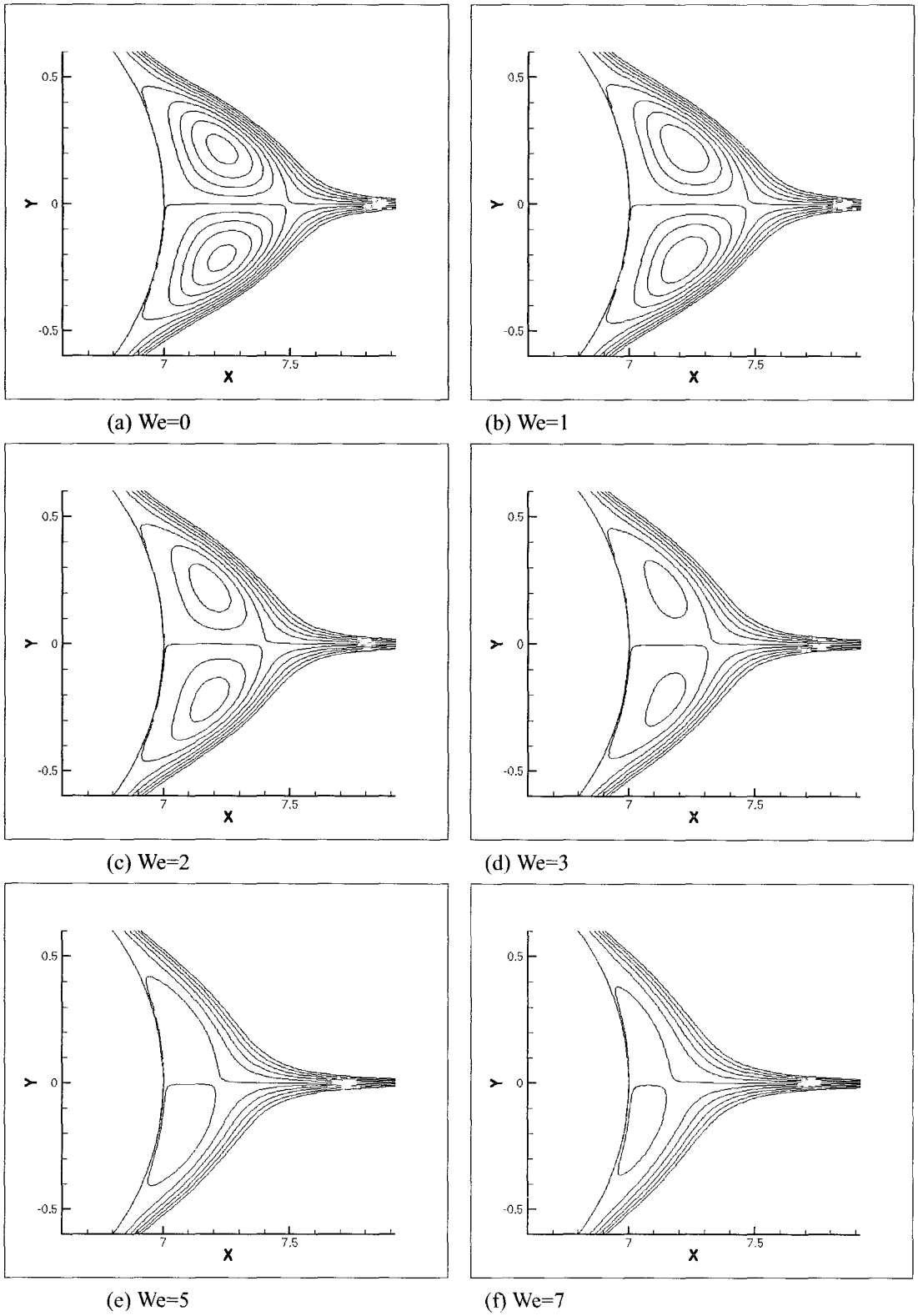

Fig. 10. Streamlines ($-0.004 \leq \psi \leq 0.004$, $\Delta\psi$=8e-4) at the rear of the cylinder when Re=10, L^2=100 and β=0.1.

may be attributed to over-predicting extensional viscosity of Oldroyd-B model.

In the present work, we have discussed the vortex behavior of flow around a confined cylinder with FENE-CR model. Even though the cylinder problem in Poiseuille flow seems to be simple, the flow behavior is rather com-

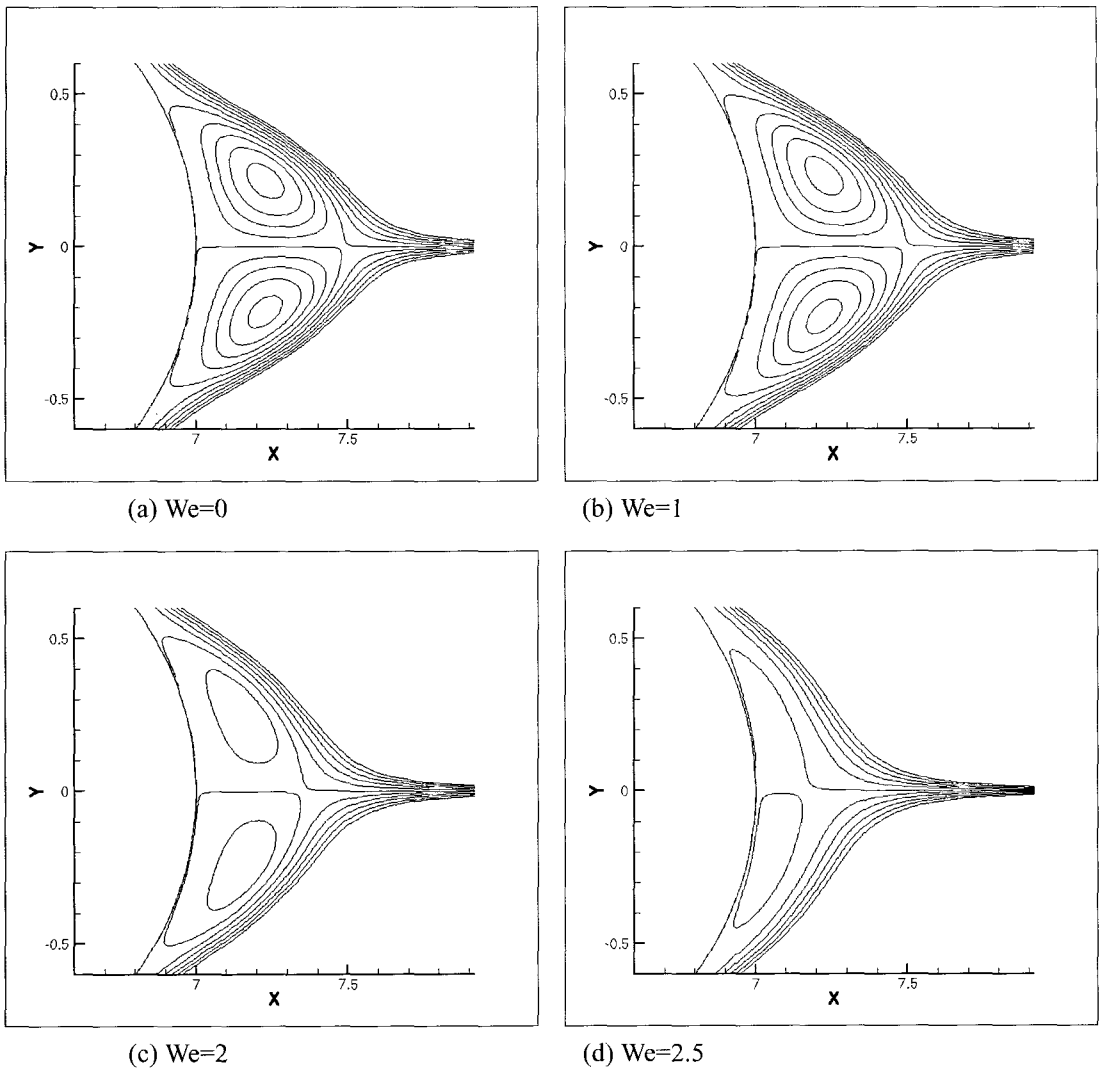

Fig. 11. Streamlines ($-0.004 \leq \psi \leq 0.004$, $\Delta\psi$=8e-4) at the rear of the cylinder when Re=10, L^2=1000 and β=0.1.

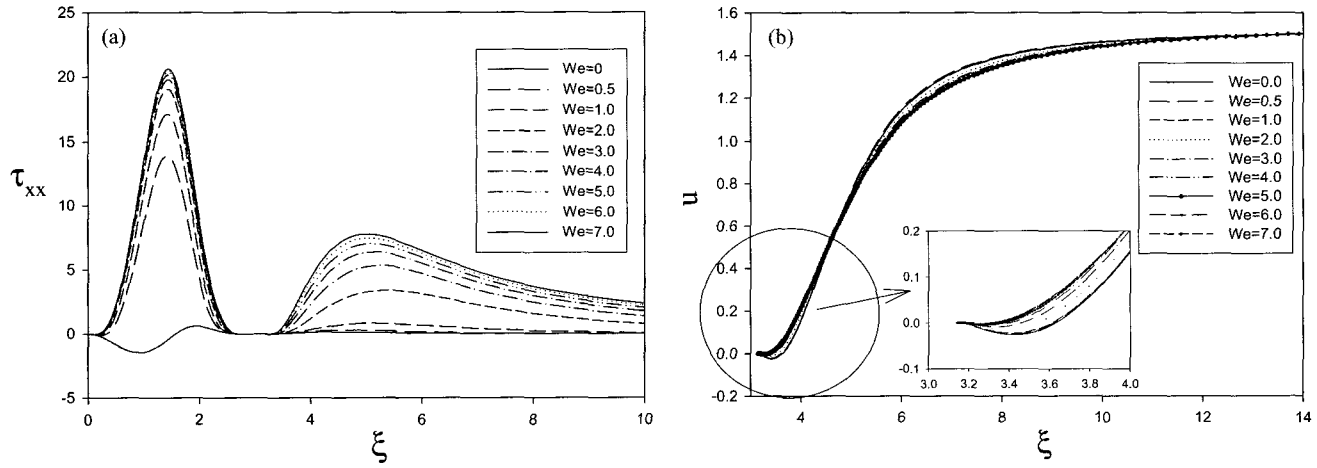

Fig. 12. Longitudinal normal stress component and velocity profiles when Re=10, β=0.1, L^2=100: (a) longitudinal normal stress component and (b) velocity profiles.

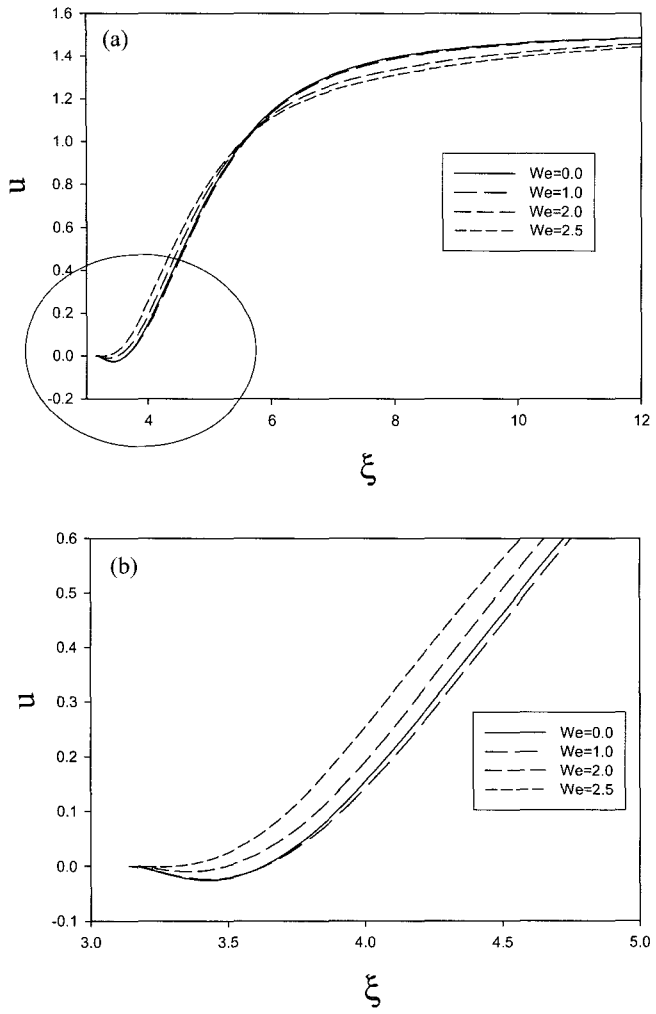

Fig. 13. Velocity profiles and its magnified view when Re=10, β=0.1, L^2=1000: (a) normal view, (b) magnified view of the circled region in (a).

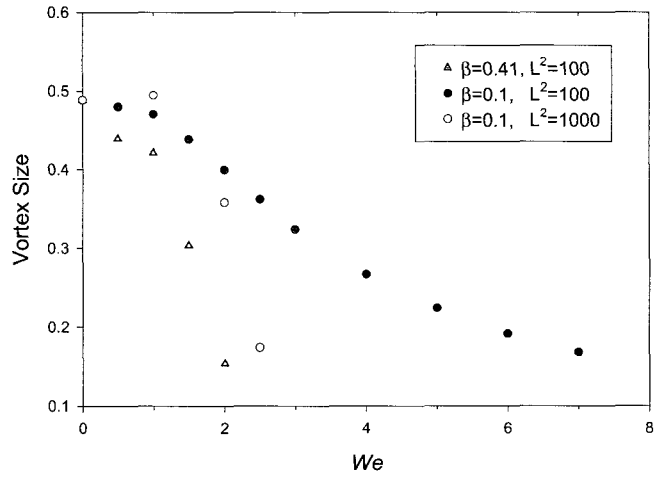

Fig. 14. Dependence of the vortex length on material parameters when Re=10.

plex. It seems that the viscoelasticity retards the formation of vortex, which is a variant of stabilization effect of viscoelasticity. In the present work, we did not investigate the shear-thinning fluid in order to exclude the shear-thinning effect. Finally, we like to point out that there is no experimental work directly related to the present study, however, the present work will be useful for understanding the inertial vortex dynamics and for future experiments.

5. Conclusions

In this work, the effect of elasticity and extensional viscosity on the steady inertial vortex dynamics has been investigated with FENE-CR model. The present study shows that the vortex dynamics is strongly dependent upon the material parameters. The reduction of vortex size was obvious for a wide range of elasticity, however, the vortex enhancement was also observed for a narrow range in case of large L^2. It is proposed that the positive longitudinal gradient of normal stress results in retarding the formation of vortex, whereas the extensional viscosity plays a role in vortex enhancement. The stabilization effect of viscoelasticity seems to be obvious at high We, however, the stabilization window is dependent upon the extensional property as well.

Acknowledgement

This work was supported by the National Research Laboratory Fund (NRL 400-20030085) of the Ministry of Science and Technology in Korea. The authors acknowledge the support from KISTI (Korea Institute of Science and Technology Information) under 'Grand Challenge Support Program' with Dr. Jeong Ho Kim as the technical supporter. The use of the computing system of Supercomputing Center is also greatly appreciated.

References

Adachi, K., N. Yoshikoka and Sakai, 1977; 1978, An investigation of non-Newtonian flow past a sphere, *J. Non-Newt. Fluid Mech.* **3**, 107-125.

Alves, M.A., F.T. Pinho and P.J. Oliveira, 2001, The flow of viscoelastic fluids past a cylinder: finite-volume high-resolution methods, *J. Non-Newt. Fluid Mech.* **97**, 207-232.

Arigo, M.T. and G.H. McKinley, 1998, An experimental investigation of negative wakes behind spheres settling in a shear-thinning viscoelastic fluid, *Rheol. Acta* **37**, 307-327.

Baloch, A., P. Townsend and M.F. Webster, 1996, On vortex development in viscoelastic expansion and contraction flows, *J. Non-Newt. Fluid Mech.* **65**, 133-149.

Broadbent, J.M. and B. Mena, 1974, Slow flow of an elastico-viscous fluid past cylinders and spheres, *Chem. Engng. J.* **8**, 11-19.

Brooks, A.N. and T.J.R. Hughes, 1982, Streamline upwind/ Petrov-Galerkin formulations for convection dominated flows

with particular emphasis on the incompressible Navier-Stokes equations, *Comput. Methods Appl. Mech. Eng.* **32**, 199-259.

Bush, M.B., 1994, On the stagnation flow behind a sphere in a shear-thinning viscoelastic liquid, *J. Non-Newt. Fluid Mech.* **55**, 229-247.

Caola, A.E., Y.L. Joo, R.C. Armstrong and R.A. Brown, 2001, Highly parallel time integration of vicoelastic flows, *J. Non-Newt. Fluid Mech.* **97**, 207-232.

Chilcott, M.D. and J.M. Rallison, 1988, Creeping flow of dilute polymer solutions past cylinders and spheres, *J. Non-Newt. Fluid Mech.* **29**, 381-432.

Christiansen, R.L., 1985, A laser-Doppler anemometry study of viscoelastic flow past a rotating cylinder, *Ind. Eng. Chem. Fundam.* **24**, 403-408.

Cressman, J.R., Q. Bailey and W.I. Goldburg, 2001, Modification of a vortex street by a polymer additive, *Phys. Fluids* **13**, 867-871.

Dou, H.-S. and N. Phan-Thien, 2003, Negative wake in the uniform flow past a cylinder, *Rheol. Acta* **42**, 383-409.

Dou, H.-S. and N. Phan-Thien, 2004, Criteria of negative wake generation behind a cylinder, *Rheol. Acta*, 1435-1528 (Online).

Fan, Y. and M.J., Crochet, 1995, High-order finite element methods for steady viscoelastic flows, *J. Non-Newt. Fluid Mech.* **57**, 283-311.

Fan, Y., R.I. Tanner and N. Phan-Thien, 1999, Galerkin/least-square finite-element methods for steady viscoelastic flows, *J. Non-Newt. Fluid Mech.* **84**, 233-256.

Harlen, O.G., 2002, The negative wake behind a sphere sedimenting through a viscoelastic fluid, *J. Non-Newt. Fluid Mech.* **108**, 411-430.

Hassager, O., 1979, Negative wake behind bubbles in non-Newtonian liquids, *Nature* **279**, 402-403.

Hu, H.H. and D.D. Joseph, 1990, Numerical simulation of vicoelastic flow past a cylinder, *J. Non-Newt. Fluid Mech.* **37**, 347-377.

Huang, P.Y. and J. Feng, 1995, Wall effects on the flow of viscoelastic fluids around a circular cylinder, *J. Non-Newt. Fluid Mech.* **60**, 179-198.

James, D.F. and A.J. Acosta, 1970, The laminar flow of dilute polymer solutions around circular cylinders, *J. Fluid Mech.* **42**, 269-288.

Kim, J.M., C. Kim, K.H. Ahn and S.J. Lee, An efficient iterative solver and high resolution computations of the Oldroyd-B fluid flow past a confined cylinder, *J. Non-Newt. Fluid Mech.* (in press).

Kim, J.M., C. Kim, C. Chung, K.H. Ahn and S.J. Lee, Comparative studies on the negative wake of FENE-CR fluid in uniform and Poiseuille flows past a cylinder (in preparation).

Koniuta, A., P.M. Adler and J.M. Piau, 1980, Flow of dilute polymer solutions around circular cylinders, *J. Non-Newt. Fluid Mech.* **7**, 101-106.

Liu, A.W., D.E. Bornside, R.C. Armstrong and R.A. Brown, 1998, Viscoelastic flow of polymer solutions around a periodic, linear array of cylinders: comparisons of predictions for microstructures and flow fields, *J. Non-Newt. Fluid Mech.* **77**, 153-190.

Manero, O. and B. Mena, 1981, On the slow flow of viscoelastic liquids past a circular cylinder, *J. Non-Newt. Fluid Mech.* **9**, 379-387.

Matallah, H., P. Townsend and M.F. Webster, 1998, Recovery and stress-splitting schemes for viscoelastic flows, *J. Non-Newt. Fluid Mech.* **75**, 139-166.

McKinley, G.H., R.C. Armstrong and R.A. Brown, 1993, The wake instability in viscoelastic flow past confined circular cylinders, *Phi. Trans. R. Soc. Lond. A* **344**, 265-304.

Mena, B. and B. Caswell, 1974, Slow flow of an elastic-viscous fluid past an immersed body, *J. Chem. Engng.* **8**, 125-134.

Oliveira, P.J., 2001, Method for time-dependent simulations of viscoelastic flows: vortex shedding behind cylinder, *J. Non-Newt. Fluid Mech.* **101**, 113-137.

Pilate, G. and M.J. Crochet, 1977, Plane flow of a second-order fluid past a submerged boundaries, *J. Non-Newt. Fluid Mech.* **2**, 323-341.

Satrape, J.V. and M.J. Crochet, 1994, Numerical simulation of the motion of a sphere in a Boger fluid, *J. Non-Newt. Fluid Mech.* **55**, 91-11.

Smith, M.D., R.C. Armstrong, R.A. Brown and R. Sureshkumar, 2000, Finite element analysis of stability of two-dimensional viscoelastic flows to three-dimensional perturbations, *J. Non-Newt. Fluid Mech.* **93**, 203-244.

Sun, J., M.D. Smith, R.C. Armstrong and R.A. Brown, 1999, Finite element method for viscoelastic flows based on the discrete adaptive viscoelastic stress splitting and the discontinuous Galerkin method: DAVSS-G/DG, *J. Non-Newt. Fluid Mech.* **86**, 281-307.

Townsend, P, 1980, A numerical simulation of Newtonian and viscoelastic flow past stationary and rotating cylinders, *J. Non-Newt. Fluid Mech.* **6**, 219-243.

Ultmann, J.S. and M.M. Denn, 1971, Slow viscoelastic flow past submerged objects, *J. Chem. Engng.* **2**, 81-89.

van der Vorst, H.A., 1992, Bi-CGSTAB: A fast and smoothly converging variant of Bi-CG for the solution of non-symmetric linear systems, *SIAM J. Sci. and Stat. Comp.* **12**, 631-634.

Wapperom, P. and M.F. Webster, 1999, Simulation for viscoelastic flow by a finite volume/element method, *Comput. Methods Appl. Mech. Engrg.* **180**, 281-304.